

A Potential Canid Large Animal Model for Cleft

BY

YENA JUN

B.S., Columbia University, 2012
D.D.S., Columbia University, 2017

THESIS

Submitted as partial fulfillment of the requirements for the degree of Master of Science in Oral Sciences in the Graduate College of the University of Illinois at Chicago, 2020

Chicago, Illinois

Defense Committee:

Dr. Christina Nicholas, Chair and Advisor
Dr. Veerasathpurush Allareddy
Dr. Lina Moreno-Urbe, University of Iowa

ACKNOWLEDGEMENTS

Dr. Nicholas

Thank you so much for being an amazing advisor to learn from and work with. I am so grateful to you for giving me the opportunity to participate in this project and for your endless support, guidance, patience, and knowledge. You have been such a big part of my life in residency and I feel lucky to have you as my mentor.

Dr. Moreno-Uribe

Thank you for giving me the opportunity to be a part of the meaningful research that you are doing.

Dr. Allareddy

Thank you for your feedback and for sharing your expertise.

Nora

This journey would not have been the same without you! Thanks for making it fun and being a supportive friend and colleague.

YJ

TABLE OF CONTENTS

| <u>CHAPTER</u> | <u>PAGE</u> |
|--|-------------|
| I. INTRODUCTION..... | 1 |
| A. Background | 1 |
| B. Purpose of the Study..... | 1 |
| C. Significance of the Study..... | 2 |
| D. Null Hypotheses | 2 |
| II. REVIEW OF THE RELATED LITERATURE..... | 3 |
| A. What Is Cleft Lip and Palate?..... | 3 |
| B. Developmental Pathogenesis | 5 |
| C. Etiology | 6 |
| D. Timeline of Cleft Treatment..... | 8 |
| E. Current Methods of Grafting..... | 10 |
| F. Tissue Engineering Approach | 11 |
| G. Animal Models for Tissue Engineering Studies..... | 13 |
| III. MATERIALS AND METHODS | 15 |
| A. Sample | 15 |
| B. 3D Slicer for Volume Rendering of Alveolar Defect Site | 15 |
| C. Geomagic Control Used for Model Smoothing and Measurements of Volume and Length | 19 |
| D. Human Cleft Data..... | 22 |
| IV. RESULTS..... | 23 |
| A. Descriptive Statistics | 23 |
| B. Comparison Between NSDTRs and Humans | 25 |
| V. DISCUSSION..... | 29 |
| VI. CONCLUSION | 33 |
| APPENDICES..... | 34 |
| Appendix A..... | 34 |
| Appendix B..... | 35 |
| Appendix C..... | 36 |
| CITED LITERATURE | 37 |
| VITA | 42 |

LIST OF TABLES

| <u>TABLE</u> | <u>PAGE</u> |
|---|-------------|
| I. VOLUME OF DEFECTS IN AFFECTED NSDTRS | 23 |
| II. HEIGHT OF DEFECTS IN AFFECTED NSDTRS | 24 |
| III. DESCRIPTIVE STATISTICS FOR NSDTR CLEFTS | 25 |
| IV. DESCRIPTIVE STATISTICS FOR HUMAN CLEFTS | 25 |
| V. MANN-WHITNEY U TESTS EVALUATING SIGNIFICANT DIFFERENCES IN VOLUME AND HEIGHT FOR ALVEOLAR DEFECTS BETWEEN NSDTR AND HUMAN GROUPS | 26 |

LIST OF FIGURES

| <u>FIGURE</u> | <u>PAGE</u> |
|--|-------------|
| 1. Diagrams illustrating the features of (A) a normal mouth and lip unaffected by an orofacial cleft; (B) unilateral cleft lip; (C) unilateral complete alveolar cleft; (D) cleft palate only; and (E) unilateral cleft lip and cleft palate. | 4 |
| 2. Diagrams depicting embryonic development of the palate at (A) 7 weeks and (B) 10 weeks | 6 |
| 3. The region of defect in the alveolar ridge for bone grafting..... | 9 |
| 4. The model of the dog cranium..... | 16 |
| 5. Four-up view showing the frontal (A), sagittal (B), and transverse (C) cross-sectional slices. Slice visibility can be toggled on during the process of filling in the defect to visualize the location on the 3D model (D). | 17 |
| 6. The rendered 3D models based on the segments that have been filled in. | 18 |
| 7. Visualization of the generated 3D models of the filled in segments within the defect sites. | 19 |
| 8. The YZ-plane used to separate the models of the left and right cleft defects into two separate files. | 20 |
| 9. (A) The model after extraneous fragments were deleted and holes were filled in. (B) The model after Mesh Doctor tool was applied to smooth the surface..... | 21 |
| 10. Calculation of height from the most inferior to superior aspects of the cleft defect. | 22 |
| 11. Box plot depicting variation in volume (mm^3) of defects in NSDTR and human ($p<0.001$). | 27 |
| 12. Box plot depicting variation in height (mm) of defects in NSDTR and human ($p<0.001$). | 28 |
| 13. Landmarks labeled on dog cranium. | 34 |
| 14. Box plot depicting variation in alveolar cleft volume (mm^3) between dogs affected by cleft palate and dogs with nasal cleft..... | 35 |
| 15. Principal component analysis explaining morphological differences between dogs affected by cleft palate and dogs with nasal cleft. | 36 |

LIST OF ABBREVIATIONS

| | |
|-------|--|
| CBCT | Cone beam computed tomography |
| CL/P | Cleft lip with or without cleft palate |
| CP | Cleft palate |
| CPO | Cleft palate only |
| NSDTR | Nova Scotia Duck Tolling Retriever |

SUMMARY

Three-dimensional bioprinting has been proposed as a promising novel approach to craniofacial regeneration, such as in the alveolar cleft reconstruction of pediatric patients with cleft defects. In order to test the safety and efficacy of experimental grafting materials, an appropriate large animal model must be established. The Nova Scotia Duck Tolling Retriever (NSDTR) was recently identified as a potential canid large animal with spontaneous alveolar clefts (Wolf et al., 2014).

The current study was conducted using the cone beam computed tomographs (CBCTs) of nine affected NSDTRs with alveolar defects. All dogs displayed bilateral clefting. 3D Slicer software was used to generate the models of each dog cranium and render the 3D models of each defect. Geomagic Control software was then used to analyze the volume and height (superoinferiorly) of the models of the alveolar defects. This data was compared with average volumetric and shape data from a human sample (n=35).

NSDTR defects were found to be superoinferiorly taller and considerably narrower mesiodistally than human clefts but absolutely larger in terms of volume. While NSDTRs may provide a sufficient model for narrow alveolar clefts, the biomechanical and physiological challenges posed by very wide cleft defects are unlikely to be well-mimicked in this model organism.

I. INTRODUCTION

Background

The current gold standard for restoring the bony defect in alveolar clefts is autogenous bone grafting, although there are limitations related to the donor sites (Khojasteh et al., 2015). Advances in biomaterials and bioprinting may soon allow for custom-printed bone grafts, such as for alveolar clefts, which incorporate cells, the synthetic or natural scaffold matrix, and signaling molecules to induce tissue regeneration in the defect site based on natural healing potential (Sears et al., 2016). Prior to *in vivo* studies in humans, a large animal model may be needed to test the safety and efficacy of tissue engineered materials. Studies of tissue engineered grafts in animals thus far have involved animals in which the defect in the alveolar bone was artificially created (Pourebrahim et al., 2013; Ruitter et al., 2011). In 2014, Wolf et al. identified Nova Scotia Duck Tolling Retrievers as a potential animal model exhibiting spontaneous alveolar clefts. Characterizing the size and shape of NSDTR alveolar clefts will help to determine whether this canid would be a suitable model for animal studies of tissue engineered alveolar graft templates. The hope is that with success in animal studies, we would transition to human clinical trials and eventually be able to routinely utilize tissue engineered technologies in the reconstruction of cleft defects.

Purpose of the Study

The purpose of the study is to characterize the volume and 3D morphology of alveolar defects in affected NSDTRs and compare with cleft defects in humans to determine if NSDTRs are a potential animal model for studying tissue engineered nasoalveolar graft templates for alveolar bone grafting.

Significance of the Study

- This study assesses alveolar defects that occur spontaneously in NSDTRs. In previous studies, alveolar clefts in animals have been created by means of a cleft creation surgery or by being congenitally induced (Kamal et al., 2017).
- This study takes quantitative measurements of the volume and dimensions of the alveolar defects of the affected NSDTRs. Only gross phenotypic characterization of the affected dogs has been done (Wolf et al., 2015).

Null Hypotheses

- Alveolar defects of affected NSDTRs have similar volume to cleft defects in humans.
- Alveolar defects of affected NSDTRs have similar 3D morphology to cleft defects in humans.

II. REVIEW OF THE RELATED LITERATURE

What Is Cleft Lip and Palate?

Cleft lip (CL) and cleft palate (CP) are congenital abnormalities of the primary palate and secondary palate, respectively, resulting from failure of fusion during embryonic development (Goodacre and Swan, 2008). Cleft defects are divided into two groups: cleft palate only (CPO) and cleft lip with or without cleft palate (CL/P) (Mossey et al., 2009). CPO is more likely to be associated with syndromes than CL/P (Goodacre and Swan, 2008). Most clefting is non-syndromic, occurring as an isolated abnormality (Dixon et al., 2011). Non-syndromic clefting is the most commonly occurring craniofacial birth defect in humans (Marazita, 2012). Clefts are classified as unilateral or bilateral and microform, incomplete, or complete based on level of involvement. An incomplete cleft refers to a small notch-like opening. A cleft is described as complete if it goes through the upper lip, upper gum tissue, palate, and into the nasal base. Usually located between the lateral incisor and canine, a complete alveolar cleft results in two palatal segments with no bony separation between the base of the nose and the front teeth (as shown in Figure 1). A cleft palate - an opening in the roof of the mouth - varies in size and may involve the soft or hard palate. A cleft affecting only the soft palate is often referred to as a submucous cleft (Fritzsche, 2009).

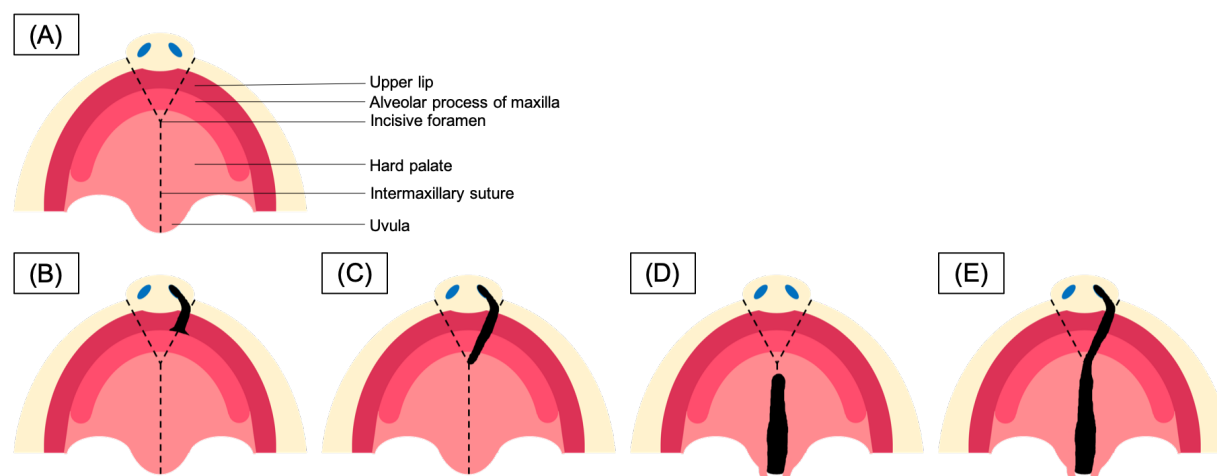


Figure 1. Diagrams illustrating the features of (A) a normal mouth and lip unaffected by an orofacial cleft; (B) unilateral cleft lip; (C) unilateral complete alveolar cleft; (D) cleft palate only; and (E) unilateral cleft lip and cleft palate.

The incidence of orofacial clefting is about 1-1.5 in 1000 live births and varies with geography and ethnicity (Tanaka, 2012). The incidence of CL/P is approximately 2 per 1000 live births among Asian Americans in the United States, while it is 1 per 1000 among Caucasians and the lowest among African Americans at 0.3 per 1000 (Fritzsche, 2009; Goodacre and Swan, 2008). Unilateral clefts are more common than bilateral clefts by a 9:1 ratio and occur twice as frequently on the left side than on the right side (Goodacre and Swan, 2008). Boys are twice as likely to be affected by CL/P than girls, and CPO is more likely to affect girls than boys by a 2:1 ratio (Dixon et al., 2011).

Orofacial clefts have complex and long-lasting medical, psychological, and social implications for children into their adulthood (Fritzsche, 2009). The primary goals in cleft care are to correct the physical defect of the lips and oral cavity and achieve the best outcome in esthetics, speech, feeding, hearing, and psychology. In addition to surgical interventions to repair clefts, children with cleft defects need multidisciplinary management from birth to adulthood. The cleft team involves plastic surgery, oral surgery, otolaryngology, dentistry,

orthodontics, nursing, speech therapy, audiology, counselling, psychology, and genetics (Moreau et al., 2007).

Developmental Pathogenesis

Clefting can occur between weeks 6 and 11 of pregnancy when there are disturbances in the complex process of craniofacial development which involves cell migration, growth, differentiation, and apoptosis (Dixon et al., 2011). Craniofacial development begins by the 4th week of human embryogenesis as neural crest cells migrate and form the frontonasal prominence, the paired maxillary processes, and the paired mandibular processes (Dixon et al., 2011). By the end of the 4th week, the formation of nasal placodes divides the frontonasal prominence into paired medial and lateral nasal processes. During the 6th week of embryogenesis, the upper lip and primary palate are formed through the merging of the medial nasal processes with each other and with the maxillary processes on each side. As the lateral nasal processes undergo peak cell division at this time, they are especially susceptible to teratogenic insults which may disrupt the closure mechanism (Mossey et al., 2009). Failure in the fusion of these processes or disturbances in growth lead to clefting of the upper lip, alveolus, and/ or primary palate (Weissler et al., 2016). Since the lip and primary palate arise from different embryonic structures than the secondary palate, cleft defects are categorized separately as CL/P or CPO.

Secondary palate development begins by the 7th week of gestation when outgrowths from the maxillary processes - the paired palatal shelves - begin growing vertically on each side of the developing tongue (Marazita, 2012). As the tongue flattens in the 7th week, the palatal shelves elevate to meet each other horizontally at the midline (as shown in Figure 2) and fuse at the midline. Differentiation of the palatal mesenchyme gives rise to the bony structures of the hard palate and muscles of the soft palate. By the 10th week of embryonic development, the

secondary palate fuses with the primary palate and nasal septum, allowing for two completely separate oral and nasal cavities. Failure in the elevation, migration, or fusion of the palatal shelves can lead to cleft defects (Mossey et al. 2009).

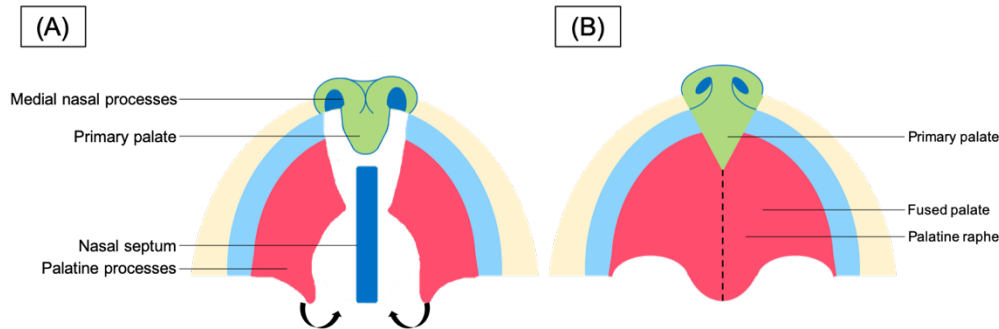


Figure 2. Diagrams depicting embryonic development of the palate at (A) 7 weeks and (B) 10 weeks.

Etiology

35% of CL/P and 54% of CPO are syndromic, meaning that the orofacial clefts occur as a component of a syndrome (Mossey et al., 2009). There are approximately 200 syndromes associated with CL/P and 400 syndromes associated with CPO, including DiGeorge syndrome, Van der Woude syndrome, Pierre Robin sequence, velocardiofacial syndrome, hemifacial microsomia/Goldenhar syndrome, and Trisomy 13 (Fritzsche, 2009). Less than 3% of syndromic clefts result from a single gene disorder (Mossey et al., 2009). Clefting is more commonly not associated with a syndrome. Isolated clefting is thought to have a multifactorial etiology involving both genetic and environmental factors (Dixon et al., 2011). Risk factors associated with clefting include smoking, anticonvulsant medications, and deficiencies in certain nutrients such as zinc, vitamin A, and folic acid (Goodacre and Swan, 2008). Smoking has consistently been found to increase the risk of CLP and CPO in a dose-response relationship (Shi et al.,

2008). Diabetes, obesity, and older maternal age have also been found to increase risk for clefts (Fritzsche, 2009).

Genetics certainly play a role in the occurrence of clefts as evidenced by the familial tendency of clefting. With regard to non-syndromic clefts, if only one parent is affected by CL/P, there is approximately a 4% chance the baby is affected; the risk increases to 17% for the second child. If neither parent has CL/P but give birth to one affected child, the risk that their second child is born with a cleft is 4%. CL/P and CPO are believed to have heterogeneous etiologies since the familial clustering and concordance recorded in twins for CL/P is different than for CPO (Mossey et al. 2009). CPO and CP/L have been found to not segregate in the same family in most cases (Dixon et al., 2011).

With regard to development of the lip and primary palate, molecular studies have identified several genes as associating with or attributing to non-syndromic clefts. The initiation and outgrowths of the facial processes may be controlled in part by the interaction of fibroblast growth factors (FGFs), sonic hedgehog (SHH), bone morphogenic proteins (BMPs); the fusion mechanism itself may be influenced by SHH, MSX1 and MSX2, and TP63 which may control signaling by BMPs and FGFs (Mossey et al., 2009). As for the development of the secondary palate, palatal growth is regulated by signaling between the palatal epithelium and mesenchyme, which includes FGF10, its receptor FGFR2b, SHH, and MSX1. The elevation of the palatal shelves is thought to be controlled by local accumulation of glycosaminoglycans, signaling molecule jagged 2 (JAG2), and interferon regulatory factor 6 (IRF6). The fusion of the palatal shelves is thought to be driven by cell-adhesion molecules, desmosomal proteins, and growth factors such as transforming growth factor α (TGF α) and TGF β 3 (Mossey et al., 2009).

While much of the genetic basis is still not well understood, recent genome-wide studies have identified specific genes and genomic regions that may increase susceptibility to cleft defects in Caucasian and Asian populations (Wolf et al., 2015). Several of the candidate genes/loci identified by linkage and association studies include BMP4, MSX1, FGFR1, and FGF8 (Leslie and Murray, 2012). Studies have also found that genes associated with syndromic clefting with a mendelian inheritance pattern can cause phenocopies of isolated clefts - one such example is IRF6, the causal gene of van der Woude syndrome, which is strongly associated with non-syndromic clefts (Leslie and Marazita, 2013).

Timeline of Cleft Treatment

Since pre-natal ultrasonography can detect cleft lip at 16 weeks gestation, cleft care can begin before birth with education and counseling for the parents. Although timing protocols vary across countries, at most North American programs, the first surgical intervention, the cheiloplasty, is done at 2 to 3 months of age to repair the lip and anterior palate. Soft palate closure is done at 4 to 12 months, once the airway is more secure (Goodacre and Swan, 2008). The second surgery is the palatoplasty to repair the cleft palate, usually at around 1 year of age. However, the timing of this procedure can vary anywhere from 6 months to 5 years due to the opposing benefits of early vs late repair (Goodacre and Swan, 2008). Early intervention to close off the nasopharynx from the oropharynx can permit better speech development, but later surgical repair minimizes the effect that palatal scarring has on restricting maxillary growth potential (James et al., 2014). Once the cleft palate repair is done, speech and language therapists can begin to evaluate and guide speech development (James et al., 2014). If needed, secondary surgery for a palatal muscle repair (a pharyngoplasty) can be done at age 3 to 5 years (James et al., 2014). Additionally, at this time, the cleft surgeon can consider nasal and lip revisions to improve cosmetics and/ or function for the child before starting school in order to minimize possible contribution to negative psychosocial interactions.

When the child is between 6 and 9 years old and in mixed dentition, the pediatric dentist and orthodontist can monitor tooth exfoliation and eruption and maxillary growth patterns. The deciduous and permanent lateral incisors are the most commonly affected teeth in children with clefts - in fact, more than half have hypodontia and one fifth have supernumerary teeth in the region (Weissler et al., 2016). Non-syndromic clefting may also result in delays in dental development of up to 1.56 years, including on the non-cleft side (Weissler et al., 2016).

Phase I orthodontics may be necessary to address maxillary growth deficiency before the child is ready for alveolar bone grafting, which is done when root formation of the permanent canine is one-half to two-thirds complete, to repair the bony deformity in the gum ridge (as depicted in Figure 3). Eruption of the permanent canine normally occurs between age 10 to 12 years. This grafting procedure involves reopening the cleft bony line and filling in the deformity with graft harvested from the iliac crest or tibial plateau (Kang, 2017). The goal in repairing the bone defect is to establish the proper arch form, for the canines erupt through the established bone graft, and to enable subsequent orthodontic management (Kang, 2017).

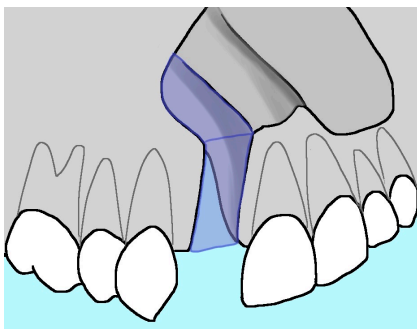


Figure 3. The region of defect in the alveolar ridge for bone grafting.

Some children with cleft who develop extreme secondary maxillary hypoplasia and suffer from negative psychosocial effects as a result may need maxillary distraction before skeletal maturity. Otherwise, orthognathic surgery can be done to address mid-face deficiency once skeletal growth has ceased, in conjunction with phase II orthodontic treatment to level and align the arches (Levy-Bercowski et al., 2011). After orthognathic surgery and alveolar grafting establish adequate nasal bony support and skeletal projection, patients may benefit from final rhinoplasty and lip revisions (James et al., 2014).

Current Methods of Grafting

Bone grafting is categorized based on when it is done, as either primary, secondary, or tertiary (Moreau et al., 2007). Timing of alveolar bone grafting depends on dental development rather than age, since dental development is often delayed and variable for children with clefts (Levy-Bercowski et al., 2011). Primary bone grafting, which is grafting that is done at or shortly after birth (within the first two years), has been shown to restrict maxillary growth and thus has largely fallen out of favor (James et al, 2014). Early secondary grafting is done between age 2 and 5 before eruption of the permanent dentition (Mahajan et al., 2017). Conventional secondary bone grafting is done at the end of mixed dentition when the canine is erupting; this is currently the most typical treatment schedule (Kang, 2017). Late secondary, or tertiary, repair is grafting that is done when the child is in full permanent dentition (Mahajan et al., 2017). Factors that have been associated with better grafting outcomes are maxillary expansion due to improved operative access, presurgical tooth extraction due to less trauma at the surgical site during the grafting procedure, and presurgical and postsurgical orthodontics (Weissler et al., 2016; Liao and Huang, 2015).

The primary goals of secondary alveolar bone grafting in cleft patients are to restore the bony defect in order to achieve maxillary stabilization and adequate nasal bony support (Pálházi et al., 2014). By establishing the proper arch form and continuity, the repair of the osseous defect can allow for tooth eruption and subsequent orthodontic treatment (Berger et al., 2014). Bone grafting also supports the upper lip and nasal cartilage and soft tissue, resulting in improvement in facial esthetics (Moreau et al., 2007). Autologous bone grafts (grafts of “donor” bone taken from another site on the patient themselves) have been the gold standard method of bony reconstruction. At least 80 percent of secondary alveolar bone grafts are considered successful, although there is some debate on what measures of outcomes are valuable (Weissler et al., 2016). The limitations of autologous grafts are donor site morbidity, limited bone availability, and postoperative pain (Kang, 2017). These drawbacks are significant, especially in cases where the initial outcome is not successful and the child needs to undergo a revision bone grafting procedure. In fact, pain at the donor site (the iliac crest) has been reported to be more severe than at the cleft site (Weissler et al., 2016). Although the outcomes of iliac crest grafting are overall good, tissue engineering has emerged as a promising alternative method for restoring alveolar cleft architecture without the disadvantages of autologous grafts (Khojasteh et al., 2015).

Tissue Engineering Approach

The goals of tissue engineering are to stimulate regeneration of tissues in defect sites and to achieve functional and esthetic outcomes. The concept of 3D printed bioscaffolds is that these scaffolds made from custom biomaterials combined with osteoinductive growth factors will guide bone regeneration by endogenous cells capable of osteogenic activity (Matsuno et al., 2010). The advantage of bioprinting over acellular scaffolds is the 3D cell distribution, which increases vascularity and nutrition for tissue regeneration (Nyberg et al., 2017). The biomaterial of choice must be biocompatible, biodegradable such that formation of new bone replaces the

resorbing graft, support cell growth and differentiation, and be mechanically stable to maintain its structural integrity (Sears et al., 2016). An additional challenge of tissue engineering in restoring the alveolus in children with cleft defects is that the scaffold must be designed to encourage ongoing growth in the child without distorting, scarring, or needing to be replaced (Moreau et al., 2007). Since materials used to bioprint have lower mechanical strength than the thermoplastic polymers used for acellular scaffolds, research has focused on improving the mechanical properties of biomaterials. Recently, composite bioscaffolds have been developed to enhance the desired properties of synthetic ceramics and natural polymers and overcome their limitations (Matsuno et al., 2010). For instance, hybrid scaffolds consisting of biodegradable polymers and biocompatible hydrogel inks have shown promise (Guvendiren et al., 2016).

In addition to biomaterials needing to exhibit the appropriate chemical and mechanical properties, the scaffold itself should be bioprintable and able to be customized in a complex 3D geometry to fit the anatomy of a patient's defect site. As a first step, 3D programs have successfully been utilized to virtually visualize patient-specific 3D templates. Pálházi and colleagues (2014) used 3D software to virtually visualize and then print 3D models of the nasoalveolar bone graft templates for 10 patients with unilateral CL and CP using their CBCTs. Berger et al. (2014) conducted an *in vitro* study in which he demonstrated the potential for cell seeding, proliferation, and osteogenic differentiation on custom 3D printed scaffolds, which were modeled with a different 3D software. One proof of concept study used 3D printed molds to fabricate cryogel scaffolds for 3D reconstructed maxillary defects and found that the cryogels accurately and nearly completely filled the molds and exhibited similar overall properties, such as mechanical durability and high pore interconnectivity, even in their complex geometric forms (Hixon et al., 2017). While these studies demonstrate successful 3D modeling and fabrication of constructs for complex architecture of alveolar ridge defects, there is a need for additional

research in developing biomaterials, printing scaffolds in complex 3D geometries with structural integrity, and understanding their performance *in vivo* (Nyberg et al., 2017).

Animal Models for Tissue Engineering Studies

In order to understand the safety and clinical effect of novel 3D bioscaffolds for cleft defects *in vivo*, we need to identify an appropriate animal model for future studies. Mice have traditionally been the most frequently studied animal model for better understanding the genetic basis human orofacial clefts (Wolf et al., 2015). However, since we want to focus on 3D scaffolds designed to fill an alveolar defect in secondary bone grafting, a limitation of the mouse model is that mice usually exhibit CPO, not CL/P. Furthermore, a larger animal model would be better suited for this task, since the size of the cleft defect would be closer to that in the human and a larger size may have different biomechanical implications which in turn may affect graft survival. In fact, the limitations of size, complexity, and tri-dimensional volume of artificially created clefts in rabbits were cited in a study that successfully reconstructed new bone in the defect sites with 3D printed bioceramic scaffolds coated with osteogenic agents (Lopez et al., 2019).

Animal models for experimental alveolar grafting have been developed by cleft creation surgery in rabbits (Kamal et al., 2017), beagle dogs (Yuanzheng et al., 2015), goats (Ruitter et al., 2011), and pigs (Caballero et al., 2015). Spontaneous cleft development *in utero* has also been shown to be possible to accomplish by feeding goats or sheep plants of the *Nicotiana* genus (Panter et al., 1990; Panter et al., 2000). The ideal animal model would exhibit spontaneous congenital cleft lip-cleft palate. Dogs have been used as models for craniofacial surgical techniques and may also be suitable models for studying tissue regeneration of cleft defects (Wolf et al., 2015). The Nova Scotia Duck Tolling Retriever was recently identified as a canid animal model with naturally occurring craniofacial defects similar to those observed in

humans with Pierre Robin Sequence (Wolf et al., 2014). This study identified a DLX6 LINE-1 insertion as the causative mutation in a subset of NSDTRs with cleft palate and mandibular abnormalities. A board certified veterinary dentist with experience in CL/P evaluation did a gross phenotypic assessment of the affected NSDTRs' clefts. Micro-computed tomography (microCT) analysis was done to further characterize the phenotypic spectrum of two NSDTRs with cleft lip and palate and syndactyly (CLPS) and three controls. In two severely affected NSDTR cases with bilateral complete CL and CP, microCT found the presence of bilateral bone and soft tissue clefts of the primary and secondary palate in the region between the incisors and canine teeth (Wolf et al., 2015).

In Wolf's 2015 study, a genome-wide association study in NSDTRs including whole-genome sequencing of three CLPS dogs and four controls led to the identification of a frameshift mutation within ADAMTS20 responsible for cleft lip in a group of affected NSDTRs (Wolf et al., 2015). A parallel GWAS done in a cohort of native Guatemalans did not find the causative mutation within ADAMTS20 but did identify four novel risk variants for CL/P with Sanger sequencing of ADAMTS20. Similar to humans, NSDTRs have been shown to exhibit molecular and phenotypic heterogeneity of orofacial clefting within the breed and therefore may be an appropriate animal model to study the repair of alveolar cleft defects using tissue engineered scaffolds (Wolf et al., 2015).

III. MATERIALS AND METHODS

Sample

Collection of data from NSDTRs were approved for Wolf's study by the University of California, Davis Animal Care and Use Committee (protocol #16892; for details on their protocols see Wolf et al., 2015). We analyzed the CBCTs of the NSDTRs with CL/P (n = 9) in this study. All dogs had bilateral clefting.

3D Slicer for Volume Rendering of Alveolar Defect Site

3D Slicer 4.6.2 was used to render the initial 3D volume of cleft defects in affected NSDTRs. An open source software platform, 3D Slicer is used by physicians and researchers for medical image informatics, image processing, and three-dimensional (3D) visualization. The files for each dog were opened to generate the 3D model of each dog (Figure 4). Since all dogs displayed bilateral clefting, we created models for both the left and right side defects.

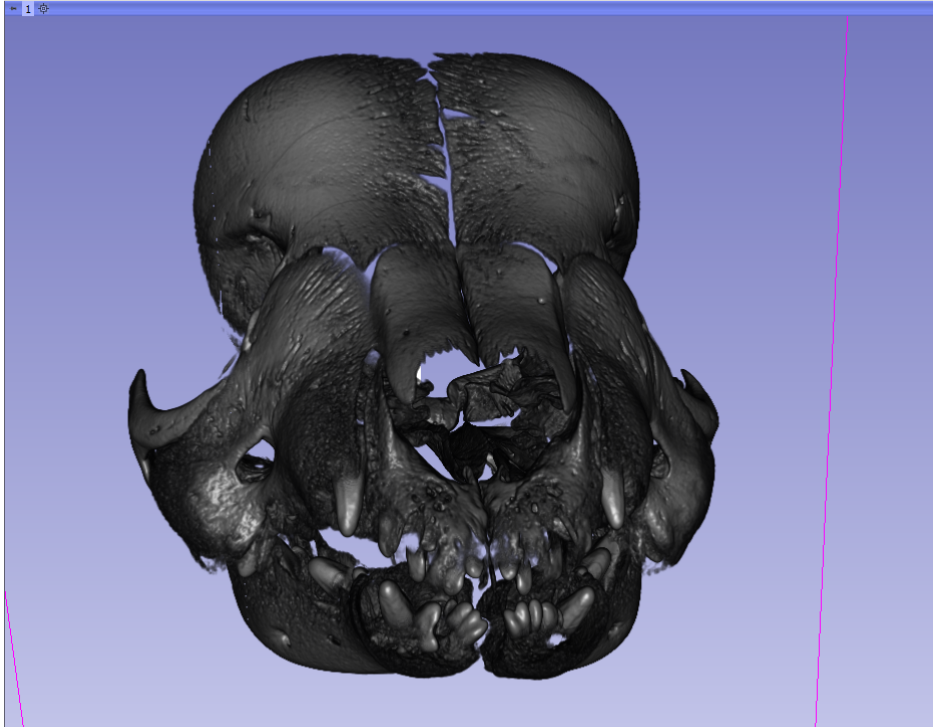


Figure 4. The model of the dog cranium.

The “four-up” view was selected for visualization of the 3D model as well as the cross-sectional slices of the model in three dimensions - sagittal, transverse, and frontal. Within each cross-sectional module, slice visibility was able to be toggled on and off to visualize the location of the cross-sectional slice on the generated 3D model; the slider was used to view the slices, occurring at 1.0 mm intervals, across the entire model (as shown in Figure 5).

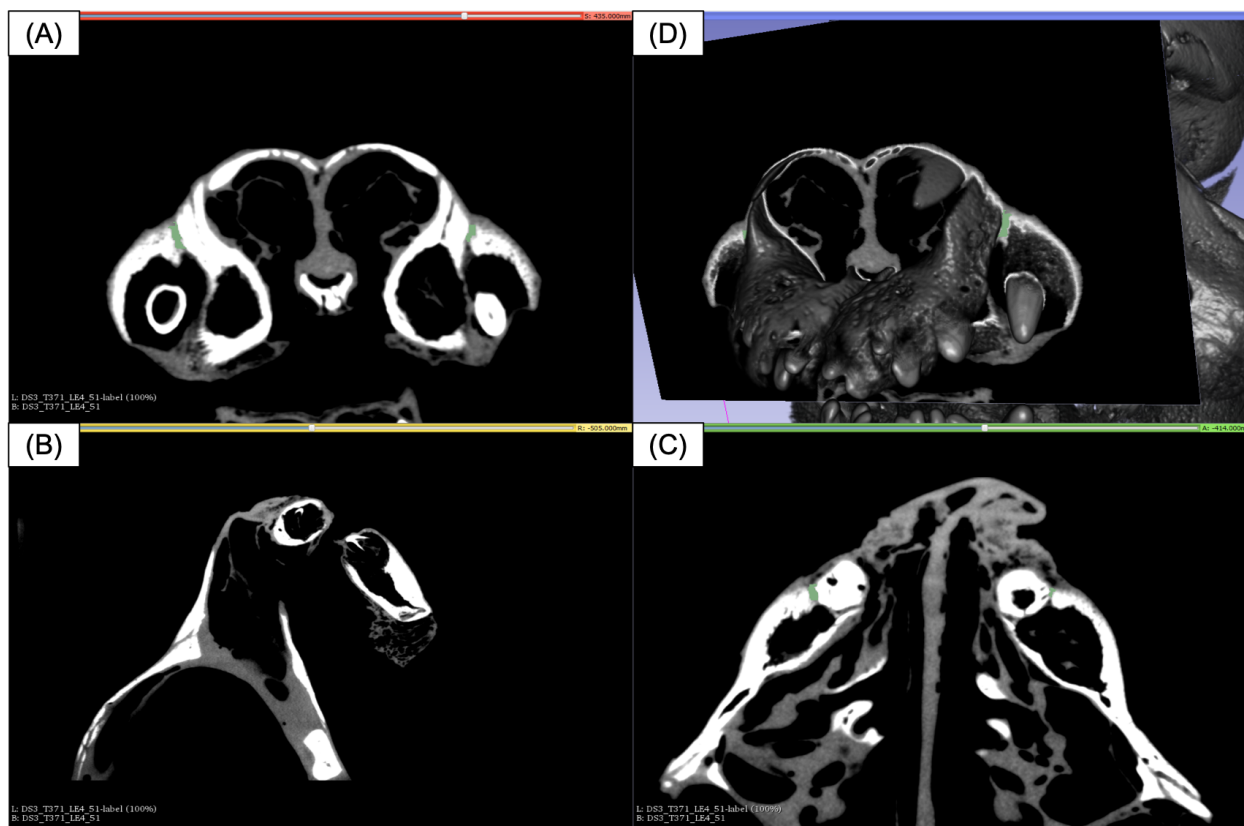


Figure 5. Four-up view showing the frontal (A), sagittal (B), and transverse (C) cross-sectional slices. Slice visibility can be toggled on during the process of filling in the defect to visualize the location on the 3D model (D).

In the Segment Editor module, the program allows for the selection of the threshold range of density for the area that will be selected. We set each threshold to exclude bone (and thus to allow us to “fill in” the area of soft tissue and open space of the defect). To create the model, a round brush was used with a diameter varying from 0.5 mm to 3 mm, adjusted according to the size of the cleft segment.

The paintbrush tool was used to “fill in” the area of the defect in each slice (moving from anterior to posterior), starting in the frontal view. The chosen threshold value prevented coloring in of the maxillary bone even if the paint tool did pass over any part of it. Once the defect was

colored in on all the appropriate frontal slices, the same segment was filled in with the paintbrush through all of the corresponding transverse slices.

After the cleft in the alveolus was filled in, the Model Maker module was used to render the 3D surface model (as shown in Figure 6) based on segmented image data - in other words, the segments that were filled in using the paint tool. The segmented models were visualized with the original model of the dog cranium to ensure that they fit smoothly (as shown in Figure 7). The adjustable parameters within the Model Maker are the number of smoothing iterations and target decimation - or reduction in the number of polygons. The corresponding sliders for these parameters were used to select a smoothen value of 15 and decimation value of 0.20 for the model creations, which were then saved as .ply files.



Figure 6. The rendered 3D models based on the segments that have been filled in.

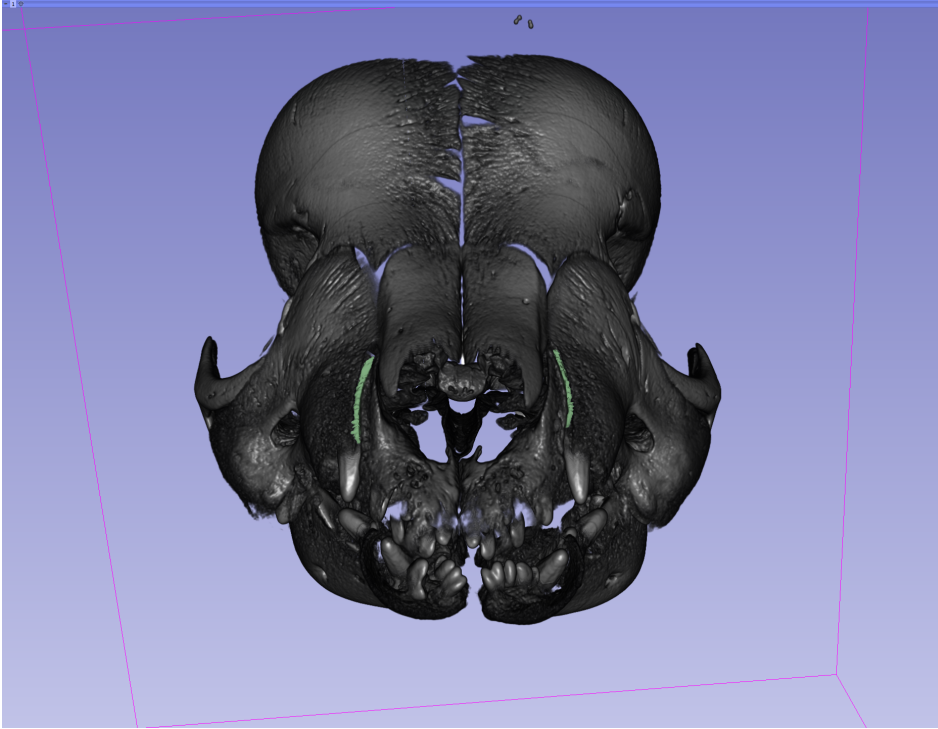


Figure 7. Visualization of the generated 3D models of the filled in segments within the defect sites.

Geomagic Control Used for Model Smoothing and Measurements of Volume and Length

The model created from 3D Slicer, a ply file, was opened in Geomagic Control 2014 for the process of fixing small holes in the models, smoothing the surface, and measuring volume and length. Under the polygons module, the file was intersected with the appropriate plane to divide the left and right models of the alveolar cleft defect (as shown in Figure 8), and the model for each side was subsequently saved as its own file in order to perform the Geomagic Control analysis individually for each model.

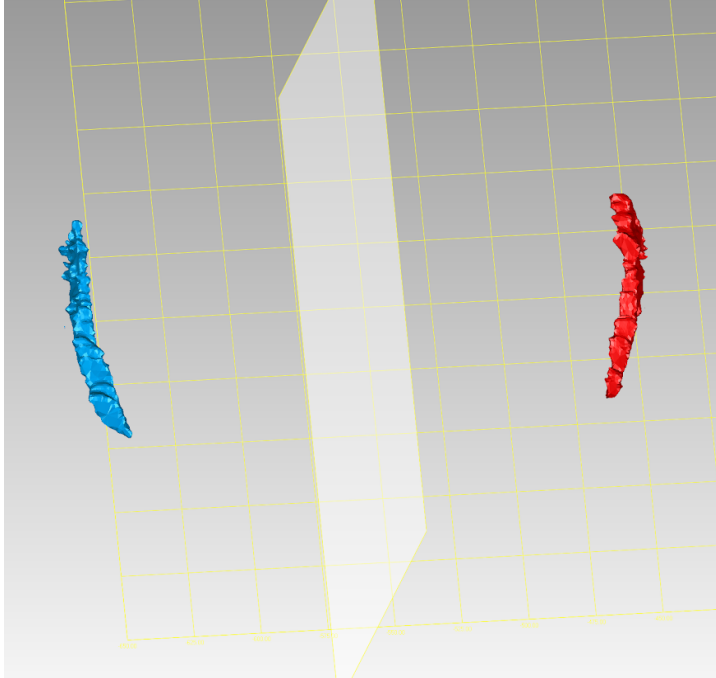


Figure 8. The YZ-plane used to separate the models of the left and right cleft defects into two separate files.

Initially the lasso tool was used to remove any extraneous fragments; for minor discontinuities in the surface of the model, the “fill single” option in the polygons module was used to fill any openings and to add a new mesh to match the curvature of the surrounding mesh. The Mesh Doctor tool was applied to each of the models to smooth the surface by removing spikes, highly creased edges, and small components and irregularities (as shown in Figure 9). The threshold for each Mesh Doctor setting was kept constant for all models.

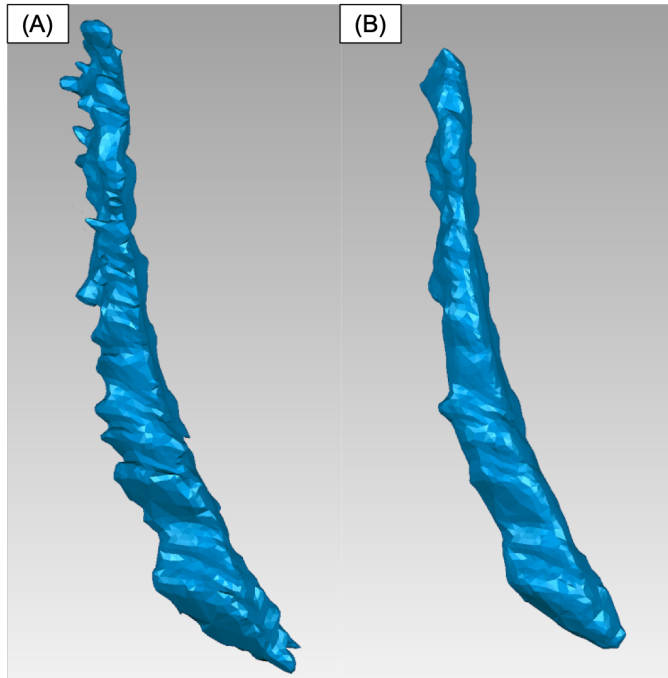


Figure 9. (A) The model after extraneous fragments were deleted and holes were filled in.
(B) The model after Mesh Doctor tool was applied to smooth the surface.

In the Analysis tab, Geomagic Control was able to compute the volume of the model in mm^3 . The height of the defect was computed automatically once two points were manually selected from the most superior and inferior aspects of the 3D volume (as shown in Figure 10).

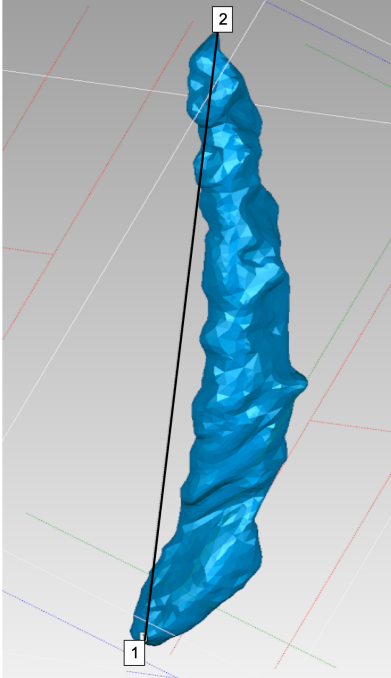


Figure 10. Calculation of height from the most inferior to superior aspects of the cleft defect.

Human Cleft Data

Bakhsh, 2020 collected data on volume and shape of clefts in a human sample (IRB: 201501711). The same methods for cleft modeling in 3D Slicer and dimension measurement in GeoMagic Control, as described above, were used for the human sample.

IV. RESULTS

Descriptive Statistics

As reported in Table I, for affected NSDTRs, the mean defect volume was determined to be 4322.50 mm³ for left side defects, 4357.31 mm³ for right side defects, and 4339.91 mm³ for all clefts. The minimum and maximum volumetric values were 614.83 mm³ and 9824.95 mm³, respectively. As reported in Table II, the mean superoinferior height was found to be 107.19 mm for the alveolar defects on the left side, 104.80 mm for defects on the right side, and 106.00 mm for all defects. The minimum and maximum height values were 57.62 mm and 149.93 mm, respectively.

TABLE I
VOLUME OF DEFECTS IN AFFECTED NSDTRS

| Dog Model | Left Side (mm ³) | Right Side (mm ³) | Mean (mm ³) |
|--------------------------------|------------------------------|-------------------------------|-------------------------|
| 1 | 1187.73 | 4122.03 | 2654.88 |
| 2 | 2755.29 | 3361.02 | 3058.16 |
| 3 | 5512.90 | 9824.95 | 7668.92 |
| 4 | 2418.37 | 2857.21 | 2637.79 |
| 5 | 3718.50 | 3370.94 | 3544.72 |
| 6 | 5872.88 | 6956.98 | 6414.93 |
| 7 | 5619.48 | 614.83 | 3117.15 |
| 8 | 7442.81 | 2585.02 | 5013.92 |
| 9 | 4374.56 | 5522.83 | 4948.69 |
| Mean Volume (mm ³) | 4322.50 | 4357.31 | 4339.91 |

TABLE II
HEIGHT OF DEFECTS IN AFFECTED NSDTRS

| Dog Model | Left Side (mm) | Right Side (mm) | Mean (mm) |
|------------------|----------------|-----------------|-----------|
| 1 | 75.65 | 141.39 | 108.52 |
| 2 | 73.91 | 80.20 | 77.05 |
| 3 | 98.51 | 108.45 | 103.48 |
| 4 | 90.40 | 86.90 | 88.65 |
| 5 | 119.45 | 96.18 | 107.82 |
| 6 | 149.93 | 148.95 | 149.44 |
| 7 | 111.88 | 57.62 | 84.75 |
| 8 | 118.18 | 107.56 | 112.87 |
| 9 | 126.81 | 115.95 | 121.38 |
| Mean Height (mm) | 107.19 | 104.80 | 106.00 |

The median volume of NSDTR defects was found to be 3920.26 mm³ and the standard deviation was 2313.02 mm³, as reported in Table III. For superoinferior height, the median was 108 mm and the standard deviation was 26 mm. The results for human clefts are reported in Table IV (for more details on the human subjects data, see Bakhsh, 2020). With regard to volume of human clefts, the mean was 783.96 mm³ with a standard deviation of 361.16 mm³, and the median was 661.01 mm³. For height, the mean was 12.18 mm with a standard deviation of 2.35 mm, and the median was 10.52 mm. For width, measured at the nasal floor, the mean was 11.62 mm with a standard deviation of 3.72 mm, and the median was 11.76 mm.

TABLE III
DESCRIPTIVE STATISTICS FOR NSDTR CLEFTS

| | Volume (mm ³) | Height (mm) |
|---------------------------|---------------------------|-------------|
| Mean | 4339.91 | 106.00 |
| Median | 3920.26 | 108.01 |
| Standard Deviation | 2313.02 | 26.18 |

TABLE IV
DESCRIPTIVE STATISTICS FOR HUMAN CLEFTS

| | Volume (mm ³) | Height (mm) | Width at the nasal floor (mm) |
|---------------------------|---------------------------|-------------|-------------------------------|
| Mean | 783.96 | 12.18 | 11.62 |
| Median | 661.01 | 10.52 | 11.76 |
| Standard Deviation | 361.16 | 2.35 | 3.72 |

Comparison Between NSDTRs and Humans

As our data was assumed not to fit a normal distribution, Mann-Whitney U tests, appropriate for non-parametric data, were used to evaluate for significant differences on the continuous dependent variables of volume and height for alveolar defects between NSDTRs and humans. The results of the Mann-Whitney U tests are reported in Table V.

TABLE V
MANN-WHITNEY U TESTS EVALUATING SIGNIFICANT DIFFERENCES IN VOLUME AND
HEIGHT FOR ALVEOLAR DEFECTS BETWEEN NSDTR AND HUMAN GROUPS

| | Volume | Height |
|-----------------------------|---------------|---------------|
| Chi-square Statistic | 28.765 | 35.679 |
| Degrees of Freedom | 1 | 1 |
| p-value | < 0.001 | < 0.001 |

The Mann-Whitney U test showed that there was a statistically significant difference in median defect volume between NSDTRs and humans, $\chi^2(1) = 28.765$, $p < 0.001$. The Mann-Whitney U test showed that there was also a statistically significant difference in median defect height between NSDTRs and humans, $\chi^2(1) = 35.679$, $p < 0.001$. The variations in volume (mm^3) and height (mm) of alveolar defects in affected NSDTRs and humans are depicted in Figure 11 and Figure 12, respectively.

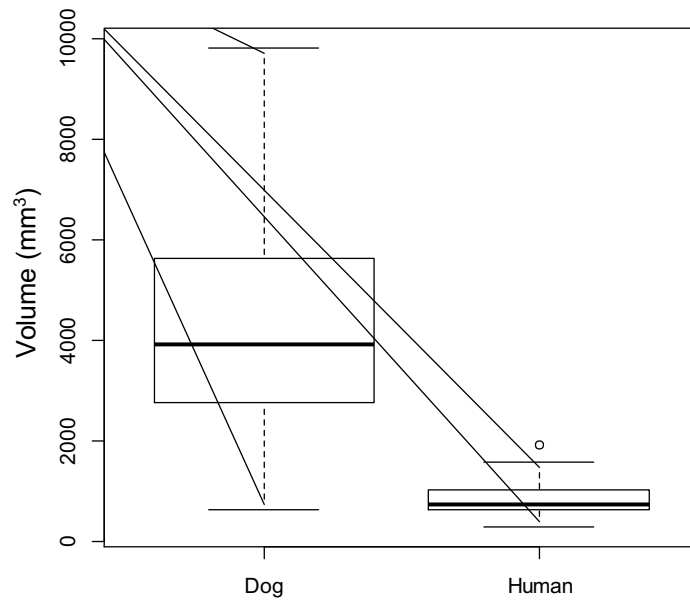


Figure 11. Box plot depicting variation in volume (mm^3) of defects in NSDTR and human ($p < 0.001$).

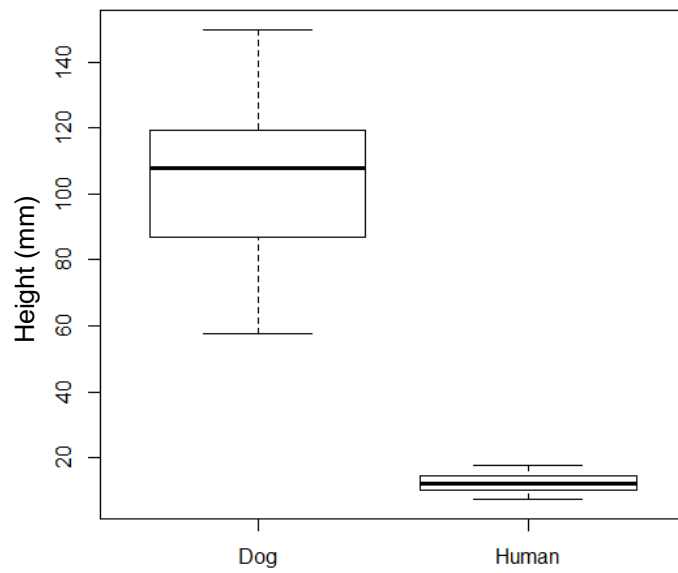


Figure 12. Box plot depicting variation in height (mm) of defects in NSDTR and human ($p < 0.001$).

V. DISCUSSION

While secondary alveolar bone grafting in the repair of cleft defects yields good outcomes, the latest advances in biomaterials and design technologies bring us closer to an alternate craniofacial regeneration approach that overcomes the challenges of autologous grafts (Nyberg et al., 2017). The 3D-bioprinting strategy seeks to create patient-specific cell-laden scaffolds for craniofacial defects of complex geometry to induce tissue regeneration (Thrivikraman et al., 2017). In the search for a safe and effective tissue-engineered strategy for alveolar cleft reconstruction, an appropriate biological model is needed to conduct testing of 3D-printed tissue analogs (Kamal et al., 2017).

Previous animal studies of 3D-bioscaffolds have used animal models with surgically-induced alveolar defects (Yuanzheng et al., 2015). Cleft models in which the alveolar defect was created and filled in a single surgery do not represent a true non-healing defect and have a bioenvironment that is different from the real clinical scenario (Kamal et al., 2017). Even for protocols that place the bone graft in a second stage surgery after epithelial lining has covered the defect, a naturally occurring cleft would most closely mimic the human environment in terms of histologic and biomechanical properties of the reconstructive scaffolds. Moreover, the animal model should have a sizeable enough skeletal defect that it is feasible to perform surgeries for clinical testing and simulates the human scenario (Lopez et al., 2019). The ideal large animal model exhibits spontaneous congenital cleft lip-cleft palate - with a defect that similar in morphology, size, and region to that of pediatric patient. The NSDTR was recently identified as a potential canid large animal with naturally occurring cleft defects (Wolf et al., 2015). Only gross phenotype of the defects has been assessed (Wolf et al., 2015); thus, this study aims to characterize the size and morphology of alveolar defects in affected NSDTRs to compare with cleft defects in humans.

The Mann-Whitney U tests found there to be a statistically significant difference in defect volume and in defect height between NSDTRs and humans ($p < 0.001$). In comparison to human clefts studied by Bakhsh, 2020, NSDTR defects were found to be absolutely larger in terms of volume but taller superoinferiorly and considerably narrower mesiodistally. With respect to cleft morphology, even the minimum recorded height measurement for an NSDTR cleft far exceeded the maximum recorded height for a human cleft. This marked difference was also true of defect width – even the widest NSDTR cleft was far narrower than the human cleft of the smallest mesiodistal width at the nasal floor. Attempts to measure defect width at the nasal floor in NSDTRs were unsuccessful because the defects tapered to a width of only several millimeters towards the most superior aspect. The alveolar defect volume in our NSDTR sample was also found to be absolutely larger when compared to cleft volume in a human sample of ten children with unilateral cleft defects (Du et al., 2017). In comparison to the average volume of NSDTR defects of 4339.91 mm^3 , the mean cleft volume in this human sample was 1.52 mL, or 1520 mm^3 .

The narrow shape of alveolar defects in NSDTRs do not well mimic the human scenario and the applicability of the results of nasoalveolar graft testing in these dogs would be compromised. Due to the biomechanical and physiological challenges posed by very wide cleft defects, NSDTRs are likely not an appropriate craniofacial model for matching the complexity of complete alveolar cleft in pediatric patients in terms of width. However, they may provide a sufficient model for the repair of narrow alveolar clefts. It is possible that the clefts represented in the above human sample were on the wider end of the spectrum since they presented after failed previous graft attempts; it may be worth investigating the prevalence and dimensions of narrow alveolar clefts. While this animal model is restricted in terms of width of defect as far as our data shows, similarities to the human clinical scenario include anatomic location of the defect, extension to the nasal floor and adjacent dentition, and non-healing status of the defect,

as opposed to some surgical animal models in which native bone healing may affect the osteogenic efficacy (Kamal et al., 2017).

This study had several limitations. One limitation was small experimental group size. Given the small sample size, the size and shape of clefts found in the affected NSDTRs included in this study may not be representative of the entire population of affected NSDTRs. Moreover, this study assessed the single breed of dog recently identified as exhibiting spontaneous alveolar clefts; future studies may identify and investigate multiple different breeds, in which cleft defects of varying size and volume may be observed. From a technical standpoint, the methods used to generate the 3D models of the defects were not a previously used standardized protocol. However, they were very similar to the process used to visualize human alveolar clefts in an image-data processing software (Pálházi et al., 2014).

To further investigate the potential of a canid large animal model for preclinical studies, future studies can characterize the volume and morphology of alveolar defects in other dog breeds that have been reported to exhibit spontaneous cleft, such as Boston Terriers or French Bulldogs (Roman et al., 2019). As discussed previously, it would also be worthwhile to assess whether clefts are narrower in a population of pediatric patients who have not had graft failure.

Although the field of bioengineering has witnessed significant breakthroughs in the development of biomaterials and technologies, there are still gaps in knowledge regarding the optimal parameters of bioprinting; for large volume bone defects, the challenge is even greater (Thrivikraman et al., 2017). In 2013, Cipitria et al. demonstrated successful bone bridging in critical-sized defects in sheep tibiae using composite scaffolds with a volume of 7916.82 mm³, printed in medical grade polycaprolactone (PCL) with β -tricalcium phosphate microparticles. With regards to the development of custom bioscaffolds for large volume alveolar bone defects

in human patients, Bartnikowski et al., 2020 demonstrated a workflow for fabricating patient specific PCL scaffolds based on CT scans for horizontal or vertical alveolar bone augmentation – the volume of 3D printed constructs ranged from 360 mm³ to 1060 mm³. If canids exhibiting naturally occurring cleft have defects within the volumetric range our study has found (from 614.83 mm³ to 9824.95 mm³), the current literature indicates that the capabilities of bioprinting are just at or below the limit of being able to handle these large volumes. Further advances in bioprinting specifically for large volume defects is likely necessary before clinical assessment in a large animal model is feasible.

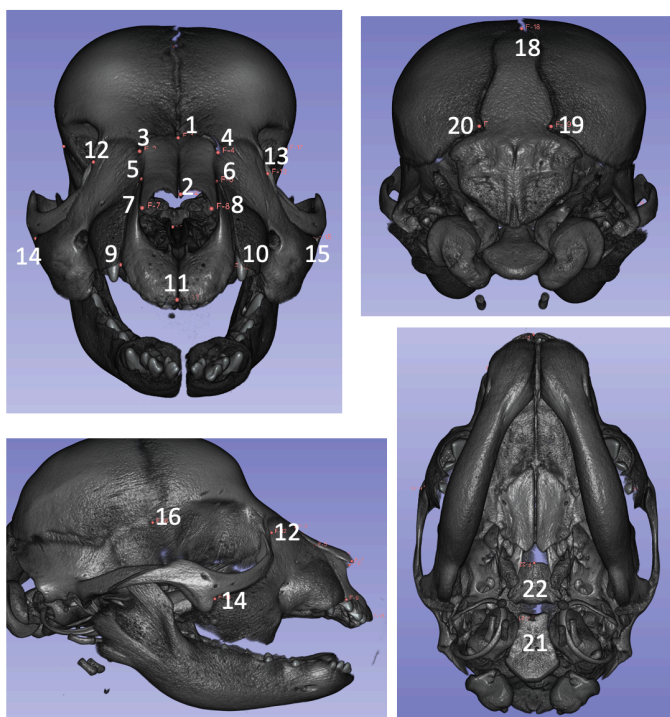
Establishing an animal model for testing tissue engineered constructs would bring us closer to exploring the potential of a novel treatment approach to alveolar cleft reconstruction in children. If animal studies can demonstrate the safety and efficacy of novel regenerative strategies for alveolar defects, these tissue engineered treatments will likely also be applicable to many other large craniofacial anomalies.

VI. CONCLUSION

According to this quantitative study evaluating the volume and shape of alveolar defects in affected NSDTRs and comparing this to the data on human clefts, we found there to be a statistically significant difference in defect volume and in defect height between NSDTRs and humans. In conclusion, we reject our null hypotheses that alveolar defects of affected NSDTRs do not have similar volume or 3D morphology to alveolar defects in humans. Therefore, NSDTRs are likely not an appropriate craniofacial model for studying tissue engineered alveolar graft templates for wide cleft defects.

APPENDICES

Appendix A



Landmarks

1. Nasion
2. Rhinion
3. Sup. Nasomaxillary suture (R)
4. Sup. Nasomaxillary suture (L)
5. Sup. Premaxillary suture (R)
6. Sup. Premaxillary suture (L)
7. Inf. Nasomaxillary suture (R)
8. Inf. Nasomaxillary suture (L)
9. Inf. Premaxillary suture (R)
10. Inf. Premaxillary suture (L)
11. Prosthion
12. Frontomaxillary suture at orbit (R)
13. Frontomaxillary suture at orbit (L)
14. Point of greatest incurvature on zygomaxillary suture (R)
15. Point of greatest incurvature on zygomaxillary suture (L)
16. Pterion (R)
17. Pterion (L)
18. Lambda
19. Point of greatest incurvature on occipital suture (R)
20. Point of greatest incurvature on occipital suture (L)
21. Basion
22. Anterior basisphenoid

Figure 13. Landmarks labeled on dog cranium.

Appendix B

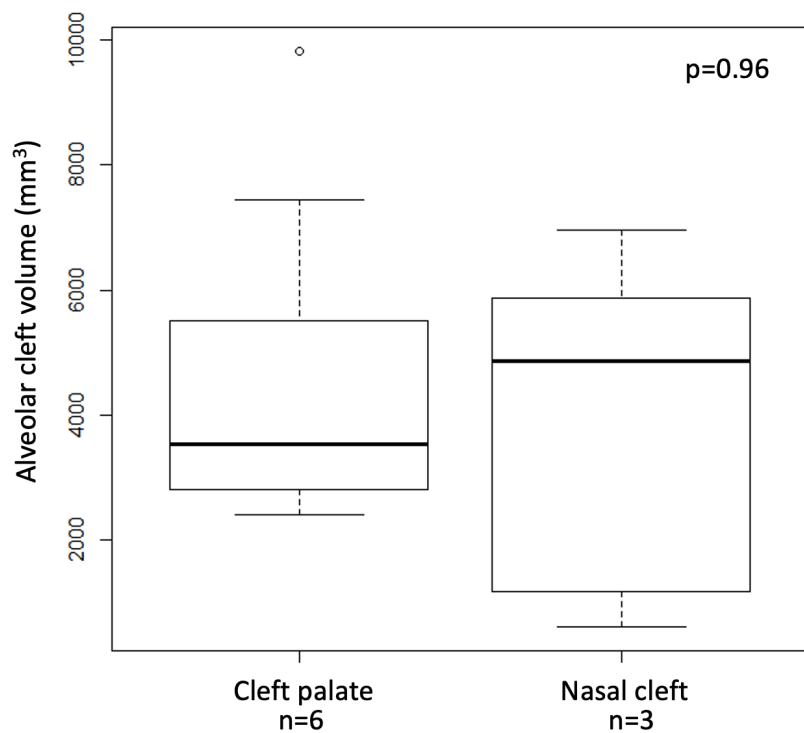


Figure 14. Box plot depicting variation in alveolar cleft volume (mm³) between dogs affected by cleft palate and dogs with nasal cleft.

Appendix C

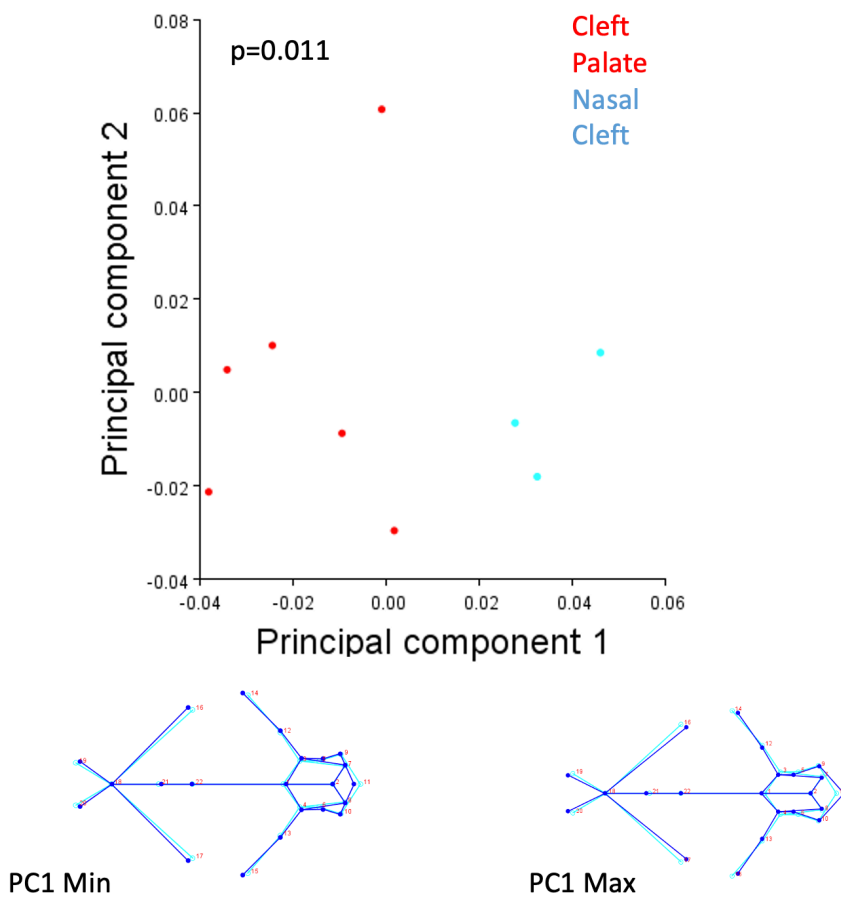


Figure 15. Principal component analysis explaining morphological differences between dogs affected by cleft palate and dogs with nasal cleft.

^aDogs with cleft palate were found to have shorter snouts and wider crania.

CITED LITERATURE

- Bakhsh, Nora. 2020. "3D Analysis of Variation in Alveolar Cleft Defect Shape and Size." MS Thesis, University of Illinois at Chicago.
- Bartnikowski, Michal, Cedryck Vaquette, and Sašo Ivanovski. n.d. "Workflow for Highly Porous Resorbable Custom 3D Printed Scaffolds Using Medical Grade Polymer for Large Volume Alveolar Bone Regeneration." *Clinical Oral Implants Research* n/a (n/a). Accessed February 3, 2020. <https://doi.org/10.1111/clr.13579>.
- Berger, Moritz, Florian Probst, Christina Schwartz, Matthias Cornelsen, Hermann Seitz, Michael Ehrenfeld, and Sven Otto. 2015. "A Concept for Scaffold-Based Tissue Engineering in Alveolar Cleft Osteoplasty." *Journal of Cranio-Maxillofacial Surgery* 43 (6): 830–36. <https://doi.org/10.1016/j.jcms.2015.04.023>.
- Caballero, Montserrat, Justin C. Morse, Alexandra E. Halevi, Omri Emodi, Michael R. Pharaon, Jeyhan S. Wood, and John A. van Aalst. 2015. "Juvenile Swine Surgical Alveolar Cleft Model to Test Novel Autologous Stem Cell Therapies." *Tissue Engineering Part C: Methods* 21 (9): 898–908. <https://doi.org/10.1089/ten.tec.2014.0646>.
- Cipitria, Amaia, Johannes C. Reichert, Devakar R. Epari, Siamak Saifzadeh, Arne Berner, Hanna Schell, Manav Mehta, Michael A. Schuetz, Georg N. Duda, and Dietmar W. Hutmacher. 2013. "Polycaprolactone Scaffold and Reduced RhBMP-7 Dose for the Regeneration of Critical-Sized Defects in Sheep Tibiae." *Biomaterials* 34 (38): 9960–68. <https://doi.org/10.1016/j.biomaterials.2013.09.011>.
- Dixon, Michael J., Mary L. Marazita, Terri H. Beaty, and Jeffrey C. Murray. 2011. "Cleft Lip and Palate: Understanding Genetic and Environmental Influences." *Nature Reviews Genetics* 12 (3): 167–78. <https://doi.org/10.1038/nrg2933>.
- Du, Fengzhou, Binghang Li, Ningbei Yin, Yilin Cao, and Yongqian Wang. 2017. "Volumetric Analysis of Alveolar Bone Defect Using Three-Dimensional-Printed Models Versus Computer-Aided Engineering." *Journal of Craniofacial Surgery* 28 (2): 383–86. <https://doi.org/10.1097/SCS.0000000000003301>.
- Fritzsche, Sharon. 2019. "Care of the Asian American Child With Cleft Lip or Palate." *Plastic Surgical Nursing* 39 (2): 35–40. <https://doi.org/10.1097/PSN.000000000000258>.
- Goodacre, Tim, and Marc C Swan. 2008. "Cleft Lip and Palate: Current Management." *PAEDIATRICS AND CHILD HEALTH*, 10.
- Guvendiren, Murat, Joseph Molde, Rosane M.D. Soares, and Joachim Kohn. 2016. "Designing Biomaterials for 3D Printing." *ACS Biomaterials Science & Engineering* 2 (10): 1679–93. <https://doi.org/10.1021/acsbomaterials.6b00121>.
- Haque, Sanjida, and Mohammad Khursheed Alam. 2015. "Common Dental Anomalies in Cleft Lip and Palate Patients." *The Malaysian Journal of Medical Sciences : MJMS* 22 (2): 55–60.

- Hixon, Katherine R, Alexa M Melvin, Alexander Y Lin, Andrew F Hall, and Scott A Sell. 2017. "Cryogel Scaffolds from Patient-Specific 3D-Printed Molds for Personalized Tissue-Engineered Bone Regeneration in Pediatric Cleft-Craniofacial Defects." *Journal of Biomaterials Applications* 32 (5): 598–611. <https://doi.org/10.1177/0885328217734824>.
- James, Jeffrey N., Bernard J. Costello, and Ramon L. Ruiz. 2014. "Management of Cleft Lip and Palate and Cleft Orthognathic Considerations." *Oral and Maxillofacial Surgery Clinics of North America* 26 (4): 565–72. <https://doi.org/10.1016/j.coms.2014.08.007>.
- Kamal, Mohammad, Lars Andersson, Rene Tolba, Alexander Bartella, Felix Gremse, Frank Hölzle, Peter Kessler, and Bernd Lethaus. 2017. "A Rabbit Model for Experimental Alveolar Cleft Grafting." *Journal of Translational Medicine* 15 (1): 50. <https://doi.org/10.1186/s12967-017-1155-2>.
- Kang, Hyun-Wook, Sang Jin Lee, In Kap Ko, Carlos Kengla, James J Yoo, and Anthony Atala. 2016. "A 3D Bioprinting System to Produce Human-Scale Tissue Constructs with Structural Integrity." *Nature Biotechnology* 34 (3): 312–19. <https://doi.org/10.1038/nbt.3413>.
- Kang, Nak Heon. 2017. "Current Methods for the Treatment of Alveolar Cleft." *Archives of Plastic Surgery* 44 (3): 188–93. <https://doi.org/10.5999/aps.2017.44.3.188>.
- Khojasteh, Arash, Lida Kheiri, Saeed Reza Motamedian, and Nasser Nadjmi. 2015. "Regenerative Medicine in the Treatment of Alveolar Cleft Defect: A Systematic Review of the Literature." *Journal of Cranio-Maxillofacial Surgery* 43 (8): 1608–13. <https://doi.org/10.1016/j.jcms.2015.06.041>.
- Leslie, E. J., and J. C. Murray. 2013. "Evaluating Rare Coding Variants as Contributing Causes to Non-Syndromic Cleft Lip and Palate." *Clinical Genetics* 84 (5): 496–500. <https://doi.org/10.1111/cge.12018>.
- Leslie, Elizabeth J., and Mary L. Marazita. 2013. "Genetics of Cleft Lip and Cleft Palate." *American Journal of Medical Genetics Part C: Seminars in Medical Genetics* 163 (4): 246–58. <https://doi.org/10.1002/ajmg.c.31381>.
- Levy-Bercowski, Daniel, Eladio DeLeon, John W. Stockstill, and Jack C. Yu. 2011. "Orthognathic Cleft—Surgical/Orthodontic Treatment." *Seminars in Orthodontics* 17 (3): 197–206. <https://doi.org/10.1053/j.sodo.2011.02.004>.
- Liao, Yu-Fang, and Chih-Sheng Huang. 2015. "Presurgical and Postsurgical Orthodontics Are Associated with Superior Secondary Alveolar Bone Grafting Outcomes." *Journal of Cranio-Maxillofacial Surgery* 43 (5): 717–23. <https://doi.org/10.1016/j.jcms.2015.03.005>.
- Lopez, Christopher D., Paulo G. Coelho, Lukasz Witek, Andrea Torroni, Michael I. Greenberg, Dean L. Cuadrado, Audrey M. Guarino, Jonathan M. Bekisz, Bruce N. Cronstein, and Roberto L. Flores. 2019. "Regeneration of a Pediatric Alveolar Cleft Model Using Three-Dimensionally Printed Bioceramic Scaffolds and Osteogenic Agents: Comparison of

- Dipyridamole and RhBMP-2." *Plastic and Reconstructive Surgery* 144 (2): 358.
<https://doi.org/10.1097/PRS.0000000000005840>.
- Mahajan, Ravi, Harish Ghildiyal, Ankit Khasgiwala, Gogulnathan Muthukrishnan, and Sukhdeep kahlon. 2017. "Evaluation of Secondary and Late Secondary Alveolar Bone Grafting on 66 Unilateral Cleft Lip and Palate Patients." *Plastic Surgery* 25 (3): 194–99.
<https://doi.org/10.1177/2292550317728035>.
- Marazita, Mary L. 2012. "The Evolution of Human Genetic Studies of Cleft Lip and Cleft Palate." *Annual Review of Genomics and Human Genetics* 13 (1): 263–83.
<https://doi.org/10.1146/annurev-genom-090711-163729>.
- Matsuno, Tomonori, Kazuhiko Omata, Yoshiya Hashimoto, Yasuhiko Tabata, and Tazuko Satoh. 2010. "Alveolar Bone Tissue Engineering Using Composite Scaffolds for Drug Delivery." *Japanese Dental Science Review* 46 (2): 188–92.
<https://doi.org/10.1016/j.jdsr.2009.12.001>.
- Moreau, Jennifer L., John F. Caccamese, Dominick P. Coletti, John J. Sauk, and John P. Fisher. 2007. "Tissue Engineering Solutions for Cleft Palates." *Journal of Oral and Maxillofacial Surgery* 65 (12): 2503–11. <https://doi.org/10.1016/j.joms.2007.06.648>.
- Mossey, Peter A, Julian Little, Ron G Munger, Mike J Dixon, and William C Shaw. 2009. "Cleft Lip and Palate" 374: 13.
- Murray, J. C. 2002. "Gene/Environment Causes of Cleft Lip and/or Palate." *Clinical Genetics* 61 (4): 248–56. <https://doi.org/10.1034/j.1399-0004.2002.610402.x>.
- Nyberg, Ethan L., Ashley L. Farris, Ben P. Hung, Miguel Dias, Juan R. Garcia, Amir H. Dorafshar, and Warren L. Grayson. 2017. "3D-Printing Technologies for Craniofacial Rehabilitation, Reconstruction, and Regeneration." *Annals of Biomedical Engineering* 45 (1): 45–57. <https://doi.org/10.1007/s10439-016-1668-5>.
- Obregon, F., C. Vaquette, S. Ivanovski, D.W. Hutmacher, and L.E. Bertassoni. 2015. "Three-Dimensional Bioprinting for Regenerative Dentistry and Craniofacial Tissue Engineering." *Journal of Dental Research* 94 (9_suppl): 143S-152S.
<https://doi.org/10.1177/0022034515588885>.
- Pálhazi, Péter, Bálint Nemes, Gwen Swennen, and Krisztián Nagy. 2014. "Three-Dimensional Simulation of the Nasoalveolar Cleft Defect." *Cleft Palate-Craniofacial Journal* 51 (5): 593–96. <https://doi.org/10.1597/13-041>.
- Panter, K. E., R. F. Keeler, T. D. Bunch, and R. J. Callan. 1990. "Congenital Skeletal Malformations and Cleft Palate Induced in Goats by Ingestion of Lupinus, Conium and Nicotiana Species." *Toxicol: Official Journal of the International Society on Toxinology* 28 (12): 1377–85. [https://doi.org/10.1016/0041-0101\(90\)90154-y](https://doi.org/10.1016/0041-0101(90)90154-y).

- Panter, K. E., J. Weinzweig, D. R. Gardner, B. L. Stegelmeier, and L. F. James. 2000. "Comparison of Cleft Palate Induction by *Nicotiana Glauca* in Goats and Sheep." *Teratology* 61 (3): 203–10. [https://doi.org/10.1002/\(SICI\)1096-9926\(200003\)61:3<203::AID-TERA8>3.0.CO;2-I](https://doi.org/10.1002/(SICI)1096-9926(200003)61:3<203::AID-TERA8>3.0.CO;2-I).
- Pourebahim, N., B. Hashemibeni, S. Shahnasari, N. Torabinia, B. Mousavi, S. Adibi, F. Heidari, and M. Jafary Alavi. 2013. "A Comparison of Tissue-Engineered Bone from Adipose-Derived Stem Cell with Autogenous Bone Repair in Maxillary Alveolar Cleft Model in Dogs." *International Journal of Oral and Maxillofacial Surgery* 42 (5): 562–68. <https://doi.org/10.1016/j.ijom.2012.10.012>.
- Roman, Nicholas, Patrick C. Carney, Nadine Fiani, and Santiago Peralta. 2019. "Incidence Patterns of Orofacial Clefts in Purebred Dogs." *PLoS ONE* 14 (11). <https://doi.org/10.1371/journal.pone.0224574>.
- Ruiter, Ad de, Gert Meijer, Titiaan Dormaar, Nard Janssen, Andries van der Bilt, Piet Slootweg, Joost de Bruijn, Linda van Rijn, and Ronald Koole. 2011. "β-TCP Versus Autologous Bone for Repair of Alveolar Clefts in a Goat Model." *Cleft Palate-Craniofacial Journal* 48 (6): 654–62. <https://doi.org/10.1597/09-219>.
- Sears, Nick A., Dhruv R. Seshadri, Prachi S. Dhavalikar, and Elizabeth Cosgriff-Hernandez. 2016. "A Review of Three-Dimensional Printing in Tissue Engineering." *Tissue Engineering Part B: Reviews* 22 (4): 298–310. <https://doi.org/10.1089/ten.teb.2015.0464>.
- Shi, Min, George L. Wehby, and Jeffrey C. Murray. 2008. "Review on Genetic Variants and Maternal Smoking in the Etiology of Oral Clefts and Other Birth Defects." *Birth Defects Research Part C: Embryo Today: Reviews* 84 (1): 16–29. <https://doi.org/10.1002/bdrc.20117>.
- Tanaka, Shoichiro A., Raman C. Mahabir, Daniel C. Jupiter, and John M. Menezes. 2012. "Updating the Epidemiology of Cleft Lip with or without Cleft Palate." *Plastic and Reconstructive Surgery* 129 (3): 511e–18. <https://doi.org/10.1097/PRS.0b013e3182402dd1>.
- Thrivikraman, Greeshma, Avathamsa Athirasala, Chelsea Twohig, Sunil Kumar Boda, and Luiz E. Bertassoni. 2017. "Biomaterials For Craniofacial Bone Regeneration." *Dental Clinics of North America* 61 (4): 835–56. <https://doi.org/10.1016/j.cden.2017.06.003>.
- Vo, T.N., S.R. Shah, S. Lu, A.M. Tataru, E.J. Lee, T.T. Roh, Y. Tabata, and A.G. Mikos. 2016. "Injectable Dual-Gelling Cell-Laden Composite Hydrogels for Bone Tissue Engineering." *Biomaterials* 83 (March): 1–11. <https://doi.org/10.1016/j.biomaterials.2015.12.026>.
- Weissler, E. Hope, Kaitlyn M. Paine, Mairaj K. Ahmed, and Peter J. Taub. 2016. "Alveolar Bone Grafting and Cleft Lip and Palate: A Review." *Plastic and Reconstructive Surgery* 138 (6): 1287–95. <https://doi.org/10.1097/PRS.0000000000002778>.

Wolf, Zena T., Harrison A. Brand, John R. Shaffer, Elizabeth J. Leslie, Boaz Arzi, Cali E. Willet, Timothy C. Cox, et al. 2015. "Genome-Wide Association Studies in Dogs and Humans Identify ADAMTS20 as a Risk Variant for Cleft Lip and Palate." Edited by Tosso Leeb. *PLOS Genetics* 11 (3): e1005059. <https://doi.org/10.1371/journal.pgen.1005059>.

Wolf, Zena T, Elizabeth J Leslie, Boaz Arzi, Kartika Jayashankar, Nili Karmi, Zhonglin Jia, Douglas J Rowland, et al. 2014. "A LINE-1 Insertion in DLX6 Is Responsible for Cleft Palate and Mandibular Abnormalities in a Canine Model of Pierre Robin Sequence." *PLOS Genetics* 10 (4): 11.

Yuanzheng, Chen, Gao Yan, Li Ting, Fu Yanjie, Wu Peng, and Bai Nan. 2015. "Enhancement of the Repair of Dog Alveolar Cleft by an Autologous Iliac Bone, Bone Marrow-Derived Mesenchymal Stem Cell, and Platelet-Rich Fibrin Mixture." *Plastic and Reconstructive Surgery* 135 (5): 1405–12. <https://doi.org/10.1097/PRS.0000000000001166>.

VITA

Name: Yena Jun

Education: B.S., Economics, Columbia University, New York, NY, 2012
D.D.S., Columbia University College of Dental Medicine, New York, NY, 2017
M.S., Oral Sciences, University of Illinois at Chicago, Chicago, IL, 2020

Professional Memberships: American Association of Orthodontists
American Dental Association
Chicago Dental Society